CHALMERS

A Cross-layered Pilot Scheme for IEEE 802.11p

Keerthi Kumar Nagalapur

Communication Systems Group
Department of Signals and Systems
CHALMERS UNIVERSITY OF TECHNOLOGY
Gothenburg, Sweden 2015

Thesis for the degree of Licentiate of Engineering

A Cross-layered Pilot Scheme for IEEE 802.11p

Keerthi Kumar Nagalapur

CHALMERS

Communication Systems Group
Department of Signals and Systems
Chalmers University of Technology

Gothenburg, Sweden 2015

Keerthi Kumar Nagalapur
A Cross-layered Pilot Scheme for IEEE 802.11p

Department of Signals and Systems
Technical Report No. R010/2015
ISSN 1403-266X

Communication Systems Group
Department of Signals and Systems
Chalmers University of Technology
SE-412 96 Göteborg, Sweden
Telephone: + 46 (0)31-772 1000
Email: keerthi@chalmers.se

This thesis has been prepared using LaTeX.

Printed by Chalmers Reproservice,
Göteborg, Sweden, October 2015.

Abstract

Vehicular communication is expected to be a part of the future transportation system and promises to support a plethora of applications for traffic safety, traffic efficiency, and fuel efficiency. Traffic safety applications, such as collision avoidance, demand reliable communications with low latency. To support reliable communications in terms of low frame error rates (FERs), it is necessary to accurately estimate the wireless channel in a receiver. Vehicular wireless channels being highly time- and frequency-variant require the communication systems to accurately estimate the channels for the entire duration of the frames. IEEE 802.11p has been specified as the physical and medium access layers standard for vehicular communications. The pilots in an 802.11p frame are densely concentrated at the beginning of the frame, and as a consequence, accurate channel estimation at later parts of the frame becomes a challenging task. To attain low FERs with the existing pilot pattern, receivers with iterative decoding and equalization strategies have been studied in the literature. These receivers are computationally complex and introduce additional latency in decoding the frames.

In this thesis, an alternative solution to overcome the ill-suited pilot pattern is studied. In Paper A, a cross-layered pilot scheme to insert complementary pilots into the 802.11p frame is proposed. The pilot insertion is performed above the physical and medium access layers and therefore does not require modifications to the 802.11p standard. A modified receiver can utilize the complementary pilots for improved channel estimation, while a standard receiver treats the inserted pilots as data and passes them to the higher layers, where they can be removed. A modified receiver that utilizes the complementary training symbols for channel estimation with linear minimum mean squared-error interpolator is described. Numerical results show that FER close to the case with perfect channel state information (CSI) can be obtained with the described receiver for suitably chosen period of pilot insertion. In Paper B, the pilot insertion scheme proposed in Paper A is further improved to support short frames. Hardware implementation feasibility of the proposed scheme is shown by implementing a modified receiver that can utilize the complementary pilots in an field programmable gate array (FPGA) platform. Two low complexity channel estimation schemes are implemented in the modified receiver. Backward compatibility of the proposed scheme is also verified by conducting tests with a commercial transceiver. FER measurements are performed by interfacing the implementation with a channel emulator. The results show that the modified receiver follows the performance of a receiver with perfect CSI with an offset of 3.5 to 4 dB in signal-to-noise ratio and significantly outperforms the commercial 802.11p transceiver we tested.

Keywords: IEEE 802.11p, Channel Estimation, Cross-layer, FPGA implementation, OFDM, Pilot Scheme

List of Publications

Included Papers

This thesis is based on the following appended papers.

[A] K. K. Nagalapur, F. Brännström, and E. G. Ström, "On channel estimation for 802.11p in highly time-varying vehicular channels," in *IEEE International Conference on Communications (ICC)*, Sydney, June 2014, pp. 5659-5664.

[B] K. K. Nagalapur, F. Brännström, E. G. Ström, F. Undi, and K. Mahler, "An 802.11p cross-layered pilot scheme for time- and frequency-varying channels and its hardware implementation," *submitted to IEEE Transactions on Vehicular Technology, Connected Vehicle Series*, Oct. 2015.

Other Work

The following patent is based on Paper [A] listed above and is not appended in this thesis.

[a] K. K. Nagalapur, F. Brännström, and E. G. Ström, "Method to introduce complementing training symbols into an 802.11p OFDM frame in vehicular communications," *International patent submitted through the Patent Cooperation Treaty (PCT)*, no. WO2015/044424, filed by Volvo Car Corporation, Sept. 2014.

Acknowledgements

This thesis would not have been possible without the guidance and support of my main supervisor Fredrik Brännström and co-supervisor Erik Ström. They have encouraged my unconventional ideas and have constantly backed me in their pursuit. I sincerely thank them and look forward to working with them in the coming years.

Thanks to all the friends and colleagues at the Communication Systems Group and the Department of Signals and Systems for creating a healthy and encouraging work environment. Many thanks to the administration staff, especially, Agneta, Natasha, and Lars, who are responsible for the smooth functioning of the department. I also take this opportunity to thank my friends outside the department, who have made the experience of living away from home, a pleasant one.

Thanks to my colleagues at Fraunhofer Heinrich Hertz Institute, Berlin for hosting me and providing me an opportunity to get hands-on experience with the practical side of communications. In particular, I am grateful to Fabian Undi for his patience in helping me with the hardware implementation.

Finally and most importantly, I would like to convey my deepest gratitude to my parents and family.

Keerthi Kumar Nagalapur
Gothenburg, October 2015

This work was funded by Chalmers Antenna Systems Excellence Center (CHASE), a VINNOVA excellence center, in the project 'Antenna Systems for V2X Communication'. Thanks to COST IC 1004 STSM and Ericsson research foundation grants for partially funding my visits to Fraunhofer Heinrich Hertz Institute, Berlin, and IEEE ICC 2014.

Acronyms

ADC	analog to digital converter
AGC	automatic gain control
AOA	angle of arrival
AOD	angle of departure
APP	a-posteriori probability
BER	bit error rate
CDP	constructed data pilot
CP	cyclic prefix
CRC	cyclic redundancy check
CSI	channel state information
DAC	digital to analog converter
DSP	digital signal processing
DSRC	dedicated short range communications
FER	frame error rate
FFT	fast Fourier transform
FPGA	field programmable gate array
GLOSA	green light optimal speed advisory
GSCM	geometry-based stochastic channel model
HDL	hardware description language
HLL	high level language
I2V	infrastructure-to-vehicle
IEEE	Institute of Electrical and Electronics Engineers
ITS	intelligent transportation systems

LLC	logical link control
LLR	log-likelihood ratio
LMMSE	linear minimum mean squared error
LOS	line-of-sight
LS	least-squares
LT	long training
MAC	medium access control
MCS	modulation and coding scheme
MF	modified 802.11p frame
MIMO	multiple input multiple output
MPC	multipath component
MSE	mean squared error
NLOS	non line-of-sight
OCB	outside the context of a basic service set
OFDM	orthogonal frequency-division multiplexing
OLOS	obstructed LOS
PAPR	peak to average power ratio
pdf	probability distribution function
PDP	power delay profile
PHY	physical
PT	pseudo training
QAM	quadrature amplitude modulation
RAM	random access memory
rms	root mean square
ROM	read only memory
RX	receiver
SF	standard 802.11p frame
SNR	signal-to-noise ratio
STA	spatial temporal averaging
TX	transmitter
US	uncorrelated scattering
V2I	vehicle-to-infrastructure

V2V	vehicle-to-vehicle
WSS	wide sense stationary
WSSUS	wide sense stationary uncorrelated scattering

Contents

Part I

Overview

Chapter 1

Introduction

1.1 Background

Active and passive safety features in vehicles have significantly improved the safety of the passengers over the last few decades and continue to do so. Optical vision and radar based technologies have been recently adopted in vehicles to monitor the immediate surroundings, and thereby prevent collisions and warn the drivers of hazardous situations. However, radar and vision based systems are limited by small coverage distance and their inability to sense vehicles that are obstructed by other obstacles. Wireless radio communications can overcome the aforementioned limitations with their ability to support communications in non line-of-sight (NLOS) scenarios over longer distances. With the goal of further improving traffic safety and enabling a wide range of applications related to traffic efficiency and fuel efficiency, wireless vehicular communications are being considered for future transportation systems.

Vehicular communications are broadly classified into vehicle-to-vehicle (V2V), vehicle-to-infrastructure (V2I), and infrastructure-to-vehicle (I2V) communications. V2V communication plays an essential role in supporting the safety applications as it enables low latency intervehicular communication without requiring the support of additional infrastructure. In V2V communications, the vehicles broadcast periodic status messages and event driven messages [1]. The periodic status messages contain position, heading, velocity, acceleration, and other details of the broadcasting vehicle. The event driven messages are broadcast to convey the occurrence of specific events, for example hard breaking. Vehicles combine the information received from other vehicles with their own to enable applications that advice the driver or even control the vehicle to a certain extent. Intersection collision warning is an important application of V2V communication, where a driver is warned about an impending collision with another vehicle which might be blinded to the driver's vision by an obstacle. As an example of nonsafety applications and I2V communications, green light optimal speed advisory (GLOSA) advises the drivers to maintain a driving speed to avoid stopping at a traffic signal [2]. This application is enabled by the broadcast of status messages by traffic signals and has been shown to reduce the fuel consumption of transport vehicles. Wireless vehicular communication

has the potential to enable a plethora of applications. An extensive list of basic set of applications supported under intelligent transportation systems (ITS) can be found in [1].

It is important to characterize the channels in which the intended communication systems will be deployed. To this end, several channel measurement campaigns, characterization, and modeling studies have been conducted [3–10]. The studies indicate that the vehicular channels are highly time- and frequency-selective, and traffic scenario dependent. For example, channels in a highway scenario and an urban intersection scenario have different characteristics. V2V channels are considered to be the most challenging for enabling reliable communications due to the mobile nature of both the transmitter and the receiver.

Standardization efforts have been made to bring vehicular communications to practice. ITS-G5 and dedicated short range communications (DSRC) standards are specified for vehicular communications in Europe and US, respectively [11, 12]. Both standards use Institute of Electrical and Electronics Engineers (IEEE) 802.11p as the physical layer with a default channel spacing of 10 MHz for safety applications. IEEE 802.11p is similar to IEEE 802.11a which was originally designed for static indoor environments. In contrast to 802.11a, outside the context of a basic service set (OCB) operation mode has been chosen as the default operation mode in 802.11p, where authentication, association, and data confidentiality services are not used [13]. The OCB operation mode is well suited for rapid broadcast communications spanning over short durations and traffic scenarios where vehicles are continuously changing their location. As an immediate consequence of operating in this mode, there is no mechanism for a receiver to acknowledge the success or failure of reception of a frame. This necessitates the vehicular communication systems to support reliable communications without the aid of retransmission strategies.

Accurate channel estimates are necessary to enable reliable communications in coherent wireless communication systems. Since 802.11a was designed to operate in static indoor environments, the pilots allocated for channel estimation are densely concentrated at the beginning of a frame. The dense concentration of the pilots at the beginning of the frame and the highly time- and frequency-varying nature of the vehicular channels makes robust channel estimation at the later parts of the frame a challenging task. Several solutions have been proposed to address this problem. The proposed solutions advocate two different approaches for performing robust channel estimation in 802.11p. In the first approach, modifications to the pilot pattern are proposed which require modifications to the standard [14–16]. In the second approach, channel estimation techniques that use decision feedback and turbo equalization are proposed, which do not require modifications to the 802.11p pilot pattern [17–24]. The frame error rate (FER) performance of the decision feedback methods is either far from the case with perfect channel state information (CSI), or in cases where performance close to the case with perfect CSI is obtained, the estimation algorithms are too complex for practical low-cost implementations with today's technology.

1.2 Objectives

The aim of this thesis is to study the channel estimation techniques for 802.11p in highly time- and frequency-varying vehicular channels. To begin with, an overview of the vehicular channels and channel models is given. This is followed by a detailed discussion of the 802.11p physical layer and the pilot pattern, which plays an important role in channel estimation. A few important channel estimation techniques that have been presented for 802.11p are then discussed with their advantages and disadvantages. Author's contribution to the problem of channel estimation, i.e., a cross-layered pilot insertion scheme to introduce complementary pilots into the 802.11p frame using layers above the physical (PHY) and medium access control (MAC) layers, is presented. The proposed scheme is backward compatible with the standard 802.11p transceivers with the requirement of a software/firmware update in higher layers. A modified receiver capable of utilizing the complementary pilots is implemented in a field programmable gate array (FPGA) prototyping platform to show the implementation feasibility of the proposed scheme.

1.3 Outline

In Chapter 2, characteristics of the vehicular channels and the channel models are discussed. Chapter 3 presents the 802.11p frame format and a few channel estimation schemes studied in the literature. Also, the proposed cross-layered pilot insertion scheme is briefly described in this chapter. The methodology and the challenges faced during the hardware implementation of the modified receiver are summarized in Chapter 4. Finally, in Chapter 5, the author's contributions are summarized.

Chapter 2

Vehicular Channels

A thorough understanding of vehicular channels is necessary to design and evaluate vehicular communication systems. This chapter discusses the characteristics of vehicular channels and gives an overview of some of the vehicular channel models.

2.1 Wireless Channels

A time-varying wideband wireless channel is represented as a time-varying impulse response $h(t, \tau)$, where t is the absolute time and τ is the delay of the multipath components (MPCs). Fourier transforming $h(t, \tau)$ with respect to τ results in the time-varying transfer function $H(t, f)$.

Wireless channels can be described in terms of three contributing factors, namely, i) path-loss, ii) shadowing, and iii) small-scale fading [25, Ch. 2]. Path-loss is the attenuation of signal power as a function of distance from the transmitter (TX), and is dependent on the carrier frequency and the propagation environments. Shadowing, also known as large-scale fading, is the attenuation of signal power caused by the obstacles between TX and receiver (RX). Constructive and destructive additions of MPCs cause signal variations over distances in the order of signal wavelengths, which is referred to as small-scale fading. Over the duration of a frame, the path-loss and shadowing are approximately constant and as a consequence, small-scale fading is the main contributor to channel variations over the duration of a frame.

The wide sense stationary uncorrelated scattering (WSSUS) assumption is commonly used to simplify the correlation functions and analysis of wideband channels. Wide sense stationary (WSS) means that the mean and the time correlation function of each tap measured at two different times, t and $t + \Delta t$, depends only on the difference Δt. Uncorrelated scattering (US) means that a multipath component with delay τ_1 is uncorrelated with all multipath components with a different delay $\tau_2 \neq \tau_1$. The US assumption results in the channel transfer function $H(t, f)$ being WSS in f [26, Sec. 6.4]. As a consequence, the time-frequency correlation function of a wideband channel under the

WSSUS assumption is given by

$$R_H(t, t+\Delta t, f, f+\Delta f) = E\{H^*(t,f)H(t+\Delta t, f+\Delta f)\} \tag{2.1}$$
$$= R_H(\Delta t, \Delta f) \tag{2.2}$$

where $E\{\cdot\}$ denotes the expectation operation. The autocorrelation functions $R_{H,\mathrm{f}}(\Delta f) \triangleq R_H(0, \Delta f)$ and $R_{H,\mathrm{t}}(\Delta t) \triangleq R_H(\Delta t, 0)$ form a Fourier transform pair with the power delay profile [25, Sec. 3.3.1-2] and Doppler power spectrum of the channel [25, Sec. 3.3.3], respectively.

Coherence bandwidth B_{coh} is the contiguous band of frequencies over which the correlation function $|R_{H,\mathrm{f}}(\Delta f)| \geq \eta_{\mathrm{f}}$. Different values of η_{f} have been used in the literature to define B_{coh}. Coherence bandwidth can be approximated in terms of the root mean square (rms) delay spread τ_{rms} and is given by

$$B_{\mathrm{coh}} \approx 1/\tau_{\mathrm{rms}}. \tag{2.3}$$

Coherence time T_{coh} is the duration over which the correlation function $|R_{H,\mathrm{t}}(\Delta t)| \geq \eta_{\mathrm{t}}$. Different values of η_{t} have been used in the literature to define T_{coh}. Coherence time can be approximated in terms of the rms Doppler spread $B_{\mathrm{D,rms}}$ and is given by

$$T_{\mathrm{coh}} \approx 1/B_{\mathrm{D,rms}}. \tag{2.4}$$

The above relations indicate the order of magnitude relation between the quantities. Different scaling factors, maximum Doppler shift $B_{\mathrm{D,max}}$ (also referred to as Doppler spread), and maximum excess delay τ_{max} are used to define coherence time and bandwidths in the literature [25–27]. Nevertheless, the important thing to note is the inverse relationships in (2.3) and (2.4).

2.2 Characteristics of Vehicular Wireless Channels

Vehicular wireless channels in V2V scenarios exhibit different characteristics in comparison to the traditional cellular channels. A major factor contributing to this difference is the heights at which the transmitter and receiver antennas are mounted. In cellular scenarios, the base station antenna is located at a greater height and there are few immediate scatterers around. Whereas, in a V2V scenario both the transmitter and receiver antennas are located at similar heights, and can be surrounded by both fixed and mobile scatterers resulting in many significant multipath components. Furthermore, transmitter, receiver, and other reflectors may be moving with high velocities in opposite directions resulting in large Doppler spreads that give rise to highly time-varying channels. A detailed account on the characteristics discussed above and their effect on communication system design is given in [3].

Geometry and physical environment of the traffic scenario, and the driving directions of the transmitter and the receiver have a huge impact on the characteristics of the vehicular channels. A strong line-of-sight (LOS) component can be present in a highway scenario, which could be completely absent in an urban intersection scenario. Doppler

spreads can vary largely depending on the relative velocities between the TX and RX, and the other vehicles [3]. Owing to the scenario specific characteristics of vehicular channels, measurements in different traffic scenarios have been conducted in several campaigns [4–10]. In [9], a local scattering function is used to analyze the channel measurements from the DRIVEWAY 2009 campaign, and to compute rms delay and rms Doppler spreads of measured channels. The rms delay and rms Doppler spreads are found to vary over a large range of values for different scenarios. Rms Doppler spreads, $B_{\mathrm{D,rms}} > 900\,\mathrm{Hz}$ and rms delay spreads, $\tau_{\mathrm{rms}} > 900\,\mathrm{ns}$ are reported, which indicate the highly time- and frequency-varying nature of vehicular channels. In [10], V2V channels are broadly classified into three groups, i) LOS: in this scenario, there exists a LOS link between TX and RX; ii) obstructed LOS (OLOS): in this situation, the LOS link between TX and RX is partially or completely blocked by another vehicle; iii) NLOS: in this scenario, the LOS link and many MPCs with significant power are completely blocked by a larger obstacle such as a building. In a traffic scenario, V2V channels can transit between the above mentioned situations. For example, in a traffic intersection the V2V channel can transit from NLOS to LOS and vice-versa.

2.3 Channel Models

In this section some vehicular channel models are described with focus on small-scale fading. Three modeling approaches are discussed, namely, i) deterministic, ii) stochastic, and iii) geometry-based stochastic. For details on path-loss and shadowing models in vehicular communications see [8, 10, 28, 29].

2.3.1 Deterministic Ray-Tracing

In ray-tracing, a ray approximation of Maxwell's equations is used along with the electromagnetic properties of the objects to compute the signal contributions at the RX. In the ray approximation, electromagnetic waves are modeled as rays and all the rays (direct ray and rays with multiple reflections) that can transfer energy from TX to RX are determined. Subsequently, the attenuation of each ray due to free space propagation and interactions with the objects is computed. The contributions of all the rays are then summed up at the RX. The ray-tracing approach can accurately simulate wireless channels at the cost of the computational complexity involved in the computation of the contribution of each ray and the requirement of accurate characterization of the electromagnetic properties of the objects in the environment.

The ray-tracing approach to simulate and study the characteristics of vehicular channels has been employed in [30], where a three-dimensional ray-tracing tool called Virtual Drive is developed. The tool allows to create different road traffic scenarios by placing typical objects according to a desired density. The tool has also been used to study the optimal placement of antennas on a vehicle in [30].

2.3.2 Stochastic Channel Models

Stochastic channel models model the long term statistics of the channels in terms of the probability distribution functions (pdfs) and correlation functions of the MPCs. Although stochastic models do not allow the simulation of a specific instance of a wireless channel, they are extensively used for analyzing the statistical performance metrics of communication systems. These small-scale fading models do not include the attenuation due to path-loss and shadowing.

The WSSUS assumption is commonly used in tapped-delay line stochastic channel models [26]. The time-varying impulse response of a tapped-delay line channel is given by

$$h(t,\tau) = \sum_{l=1}^{L} a_l(t)\delta(\tau - \tau_l),$$

where L is the number of taps, $a_l(t)$ and τ_l are the time-varying complex coefficient and delay of the lth tap, respectively; and $\delta(\cdot)$ is the Dirac delta function. A pdf and autocorrelation function are assigned to each time-varying tap $a_l(t)$, and the average power of the taps is chosen according to a power delay profile (PDP).

In [6], tapped-delay line channel models for six different V2V traffic scenarios have been developed based on measurements. The models describe each tap with either a Rayleigh or Rician fading distribution and a Doppler power spectrum. Both WSSUS and non-WSSUS stochastic channel models based on measurements are developed in the form of tapped delay line models in [7]. The nonstationarity of the channel taps is modeled using 'persistence processes,' where certain taps are turned on and off according to a two state Markov process. Tap correlation coefficient matrices are specified to account for the correlation between the taps. Although vehicular channels have been shown to exhibit non-WSSUS characteristics [7, 31], they can be regarded as WSSUS over the duration of a frame allowing the use of WSSUS tapped-delay models for performance evaluation. However, the non-WSSUS characteristic of the channels prevents the collection of long term channel statistics in a receiver to facilitate channel estimation.

A time-varying transfer function of one realization of the Highway NLOS stochastic channel model based on channel measurements [32, 33] is shown in Figure 2.1. The channel has a bandwidth of 10 MHz and spans over a duration of 1.4 ms. The Highway NLOS channel model has a maximum Doppler shift $B_{\mathrm{D,max}} = 886\,\mathrm{Hz}$ and maximum excess delay $\tau_{\max} = 700\,\mathrm{ns}$, exhibiting high time and frequency selectivity as seen in the figure.

2.3.3 Geometry Based Stochastic Channel Models

The ray-tracing approach is computationally complex and the tapped-delay line models are not well suited for simulating a specific channel realization. Geometry-based stochastic channel models (GSCMs) allow simulation of a specific channel realization with reduced complexity. In GSCMs, scatterers are placed randomly according to specified statistical distributions and different scattering properties are assigned to them. Simplified ray-tracing is then used to determine the signal contribution of the scatterers

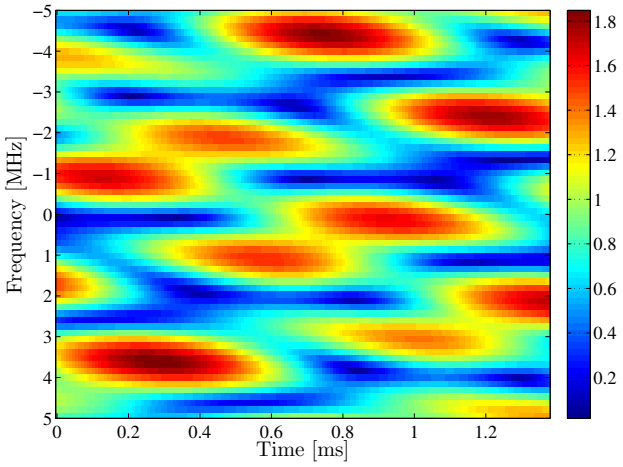

(a) Magnitude

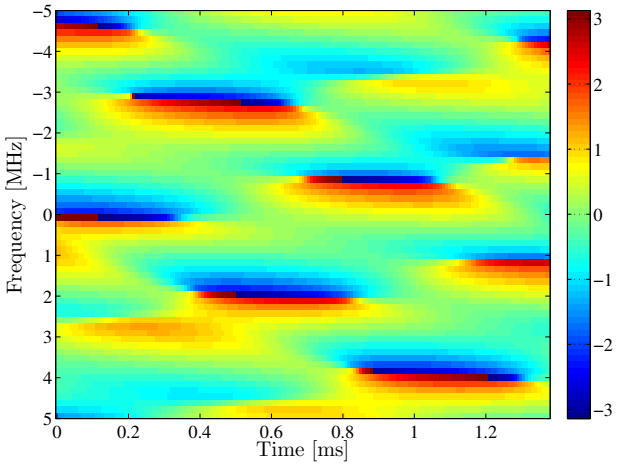

(b) Phase in radians

Figure 2.1: Time-varying transfer function $H(t, f)$ of one instance of the Highway NLOS channel in a time-frequency grid with 10 MHz bandwidth and spanning a duration of 1.4 ms.

at the receiver. Typically, only single or double scattering is considered, which greatly reduces the computational complexity [34]. GSCMs offer several benefits: (i) they can handle non-WSSUS channels, (ii) multiple input multiple output (MIMO) properties of the channel can easily be incorporated, and (iii) they provide double directional description of the channel by allowing angle of arrival (AOA) and angle of departure (AOD) description of the signal contributions, and the option of including antenna patterns.

A double directional MIMO GSCM with a detailed implementation procedure is described in [34]. The double directional, time-variant channel response is modeled as [35]

$$h(t,\tau) = \sum_{i=1}^{N} a_i(t) e^{j\frac{2\pi}{\lambda} d_i(t)} \delta(\tau - \tau_i)\delta(\Omega_R - \Omega_{R,i})\delta(\Omega_T - \Omega_{T,i}) g_R(\Omega_R) g_T(\Omega_T), \qquad (2.5)$$

where $\tau_i, \Omega_{R,i}$, and $\Omega_{T,i}$ are the excess delay, AOA and AOD of the ith path; $g_T(\Omega_T)$ and $g_R(\Omega_R)$ are the TX and RX antenna radiation patterns, respectively; $a_i(t)$ and $d_i(t)$ are the complex amplitude and the distance of the ith path, λ is the wavelength, and $e^{j\frac{2\pi}{\lambda} d_i(t)}$ is the distance-induced phase shift. In [34], the impulse response is categorized into four parts based on different types of scatterers: (i) the LOS component which might also include other static components, (ii) discrete components resulting from mobile objects (MD), (iii) discrete components resulting from static objects (SD), and (iv) diffuse components (DI). The impulse response in (2.5) is then split in four parts as

$$h(t,\tau) = h_{\mathrm{LOS}}(t,\tau) + \sum_{p=1}^{P} h_{\mathrm{MD},p}(t,\tau) + \sum_{q=1}^{Q} h_{\mathrm{SD},q}(t,\tau) + \sum_{r=1}^{R} h_{\mathrm{DI},r}(t,\tau), \qquad (2.6)$$

where P, Q, and R are the number of discrete mobile objects, discrete static objects, and diffuse components, respectively. The complex amplitudes in the four different parts are modeled using distance dependent gains and fading distributions which can be determined from channel measurements [34].

2.4 Conclusion

Relevant channel models have to be chosen to evaluate the performance of vehicular communication systems. Although ray-tracing and GSCM models can model the vehicular channels more accurately than the stochastic channel models, stochastic channel models with WSSUS assumption are still relevant for evaluating the performance of vehicular communication systems as they can be easily simulated and interfaced with transceiver implementations. Also, commercial channel emulators support emulation of stochastic channels which enable us to conduct FER performance tests on hardware transceiver implementations operating in real time. Considering these advantages, stochastic channel models are used in the thesis and the attached papers to evaluate the performance of different channel estimation algorithms.

Chapter 3

Channel Estimation in IEEE 802.11p

Channel estimation in a communication system is constrained by the modulation parameters, pilot pattern, and the channels over which they are deployed. In this chapter, the IEEE 802.11p standard and its pilot pattern are discussed. Subsequently, an overview of the channel estimation schemes that have been studied for 802.11p is given. A modified frame format with complementary pilots which is obtained by the backward standard-compatible cross-layered pilot insertion scheme proposed in the appended papers [33, 36] is introduced. To conclude, a comparison of different channel estimation schemes is given.

3.1 IEEE 802.11p

The PHY layer of 802.11p uses orthogonal frequency-division multiplexing (OFDM) with $N = 64$ subcarriers and a cyclic prefix (CP) of $N_{\mathrm{CP}} = 16$ samples. Channel spacing of 10 MHz is specified for safety related applications [37]. The parameters of 802.11p for 10 MHz channel spacing are shown in Table 3.1. The sample duration T_{S} is the minimum spacing between the samples for the 10 MHz channel spacing. The orthogonality duration (T) is the duration over which the subcarriers are orthogonal and the subcarrier spacing (Δ_f) is the separation of the subcarriers in frequency. The total duration of an OFDM symbol (T_{SYM}) is the sum of the orthogonality duration (T) and the duration of the cyclic prefix (T_{CP}).

Two guidelines are normally followed in the design of an OFDM system. Firstly, the duration of the cyclic prefix T_{CP} has to be greater than the maximum excess delay of the wireless channel $\tau_{\max}$ to completely eliminate intersymbol interference between consecutive OFDM symbols [38, Sec. 1.4], i.e.,

$$\tau_{\max} < T_{\mathrm{CP}} = 1.6\,\mu\mathrm{s}.$$

Secondly, the subcarrier spacing Δ_f has to be much larger than the maximum Doppler

Table 3.1: Parameters of IEEE 802.11p in 10 MHz channel spacing

Parameter	Symbol	Value
Sample period	T_{S}	$0.1\,\mu$s
Number of subcarriers	N	64
Orthogonality duration	T	$6.4\,\mu$s
Number of CP samples	N_{CP}	16
Duration of cyclic prefix	T_{CP}	$1.6\,\mu$s
Total symbol duration	T_{SYM}	$8\,\mu$s
Subcarrier spacing	Δ_f	156.25 kHz

shift $B_{\mathrm{D,max}}$ to keep the intercarrier interference negligible [38, Sec. 2.2], i.e.,

$$B_{\mathrm{D,max}} \ll \Delta_f = 156.25\,\mathrm{kHz}.$$

The maximum excess delay values and the Doppler shifts reported in the channel measurement campaigns [6, 7, 9] satisfy the above two guidelines for the 10 MHz channel spacing.

The encoding process of an 802.11p OFDM symbol is described in [13, 36]. The 802.11p standard supports eight different modulation and coding schemes (MCSs) for encoding the data bits. The MCS with code rate 1/2 and QPSK modulation is specified for safety applications and will be the focus of the thesis unless mentioned otherwise. Pilot symbols that are known to receivers are multiplexed with the data symbols to aid in channel estimation. Figure 3.1 shows a standard 802.11p frame (SF) in a subcarrier-time grid. Two identical OFDM symbols referred to as long training (LT) are at the beginning of the frame. The SIGNAL symbol carries the information regarding the length of the packet, and the MCS used for encoding the data bits. The DATA OFDM symbols follow the SIGNAL symbol and each of them carry four pilots referred to as comb pilots. The frame also consists of 10 short identical sequences that precede the LT symbols (not shown in figure), these are used by the receiver for frame detection, synchronization, and automatic gain control.

At the receiver, the CP of the received time domain OFDM symbol is discarded and an N-point DFT is performed to obtain the frequency domain symbols. Assuming perfect frequency and time synchronization, and that the duration of the CP is longer than the channel impulse response, the received frequency domain symbols after the DFT operation are given by [39, Sec. 8.3]

$$y[m,k] = h[m,k]x[m,k] + w[m,k], \tag{3.1}$$

where $h[m,k]$ is the channel frequency response at the kth subcarrier of the mth OFDM symbol and $w[m,k]$ is the frequency domain independent and identically distributed complex additive white Gaussian noise sample with zero mean and variance N_0. The effect of intercarrier interference is neglected since the channel can be considered to be approximately time-invariant over the duration of one OFDM symbol. The relation can

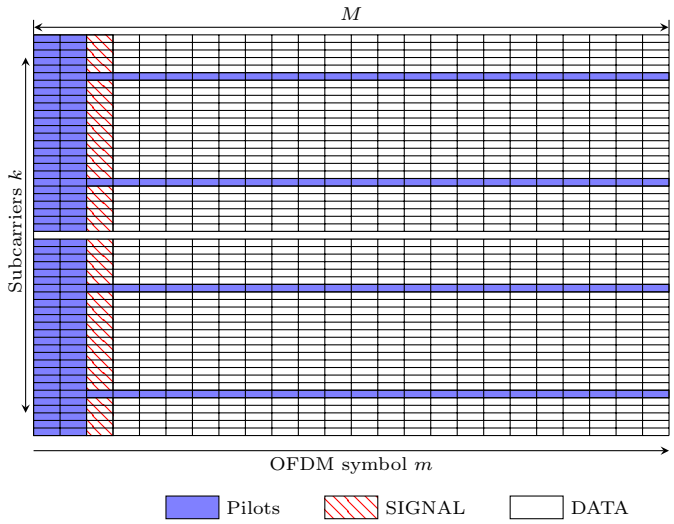

Figure 3.1: A standard 802.11p frame in subcarrier-time grid showing the position of the pilots and the data symbols.

be further written in vector notation as

$$\boldsymbol{y}_m = \boldsymbol{X}_m \boldsymbol{h}_m + \boldsymbol{w}_m, \tag{3.2}$$

where $\mathbf{X}_m$ is a diagonal matrix of transmitted quadrature amplitude modulation (QAM) symbols in the mth OFDM symbol; $\boldsymbol{h}_m$ and $\boldsymbol{w}_m$ are the column vectors of the channel frequency responses and noise samples in the mth OFDM symbol, respectively.

An estimate of the channel frequency response $h[m, k]$ is necessary to perform coherent detection. Practical wireless communication systems utilize pilot symbols to perform channel estimation. Pilots that are suitably placed in the subcarrier-time grid enable channel estimation with low mean squared error (MSE) using low complexity algorithms [40]. As seen in Figure 3.1, in 802.11p the pilots sample the channel frequency response $h[m, k]$ at all subcarriers only at the beginning of the frame and at four comb pilot subcarriers for the rest of the frame. This pilot pattern is well suited for static indoor environments for which the 802.11a was originally designed. When the channel is static, it is only necessary to estimate the channel at all the subcarriers in the beginning of a frame and use it for decoding the data in the rest of the frame. The comb pilots can be additionally used to correct slow phase or frequency drifts. Availability of channel estimates at the beginning of a frame eliminates the need for buffering of data symbols and simplifies receiver implementation. Owing to these aspects, the pilot pattern in 802.11p is an efficient design for static indoor environment.

As discussed in Chapter 2, vehicular channels are not static and if channel estimation is to be performed by using pilots, the pilots should be placed according to the coherence time and coherence bandwidth of the wireless channel. The maximum pilot separation

in frequency domain (in number of subcarriers) should satisfy

$$\Delta_{\mathrm{p},f} \leq \frac{B_{\mathrm{coh}}}{\Delta_f} \approx \frac{1/\tau_{\mathrm{rms}}}{\Delta_f}, \tag{3.3}$$

and the separation of pilots in time domain (in number of OFDM symbols) should satisfy

$$\Delta_{\mathrm{p},t} \leq \frac{T_{\mathrm{coh}}}{T_{\mathrm{SYM}}} \approx \frac{1/B_{\mathrm{D,rms}}}{T_{\mathrm{SYM}}}. \tag{3.4}$$

The requirements in (3.3) and (3.4) give insight into a suitable choice of pilot spacing based on coherence time and coherence bandwidth. They are not, however, absolute requirements.

Rms Doppler spreads, $B_{\mathrm{D,rms}} > 900\,\mathrm{Hz}$ and rms delay spreads, $\tau_{\mathrm{rms}} > 900\,\mathrm{ns}$ have been reported from the channel measurements [9, Table II]. For these values, the above mentioned conditions are not satisfied for the 802.11p pilot pattern, where $\Delta_{\mathrm{p},f} = 14 > (B_{\mathrm{coh}}/\Delta_f) \approx 7$, and no pilots are present on the data subcarriers after the LT symbols. As a consequence, estimation of vehicular channels in 802.11p becomes a challenging task.

Several solutions have been proposed to address the problem of channel estimation in 802.11p systems in highly time- and frequency-varying channels. A set of solutions propose different pilot patterns that provide more support for channel estimation and thereby require changes in the 802.11p PHY layer specification [14–16]. The other set of solutions employ decision feedback and turbo equalization techniques to improve the FER performance of the receiver while utilizing the existing pilot pattern [17–24].

3.2 Channel Estimation Schemes

Channel estimation in OFDM communication systems is a well researched topic [38, 40–46]. However, channel estimation in 802.11p OFDM systems is constrained by the pilot pattern that is ill-suited for highly time- and frequency-varying channels. In this section, some important channel estimation schemes relevant for the 802.11p systems are presented.

Channel estimation schemes are broadly classified into blind, pilot aided, and decision directed. Pilot aided estimation schemes rely on the data known at the receiver for channel estimation. Decision directed methods rely on the pilots for initial channel estimation and on the bit or constellation symbol decisions afterwards for updating the initial channel estimates. Blind channel estimation schemes do not rely on the pilots and are seldom used in practical systems due to the difference in the computation effort and the reliability offered by them, and hence not studied in this section [26, Sec. 16.7].

3.2.1 Pilot Aided Estimation

In block least-squares (LS) scheme, LS channel estimates are calculated using the two identical LT symbols and are averaged to obtain less noisy channel estimates given by

$$\hat{\boldsymbol{h}}_{\mathrm{LT-LS}} = \boldsymbol{X}_{\mathrm{LT}}^{-1}\left(\frac{\boldsymbol{y}_1 + \boldsymbol{y}_2}{2}\right), \tag{3.5}$$

where $\boldsymbol{y}_1$ and $\boldsymbol{y}_2$ are the two received LT symbols, and $\boldsymbol{X}_{\mathrm{LT}}$ is a diagonal matrix of BPSK pilot symbols in one LT OFDM symbol.

The block linear minimum mean squared error (LMMSE) channel estimates which are obtained by smoothing the LS estimates are given by [41, 44]

$$\hat{\boldsymbol{h}}_{\mathrm{LT-LMMSE}} = \boldsymbol{R}_{hh}\left(\boldsymbol{R}_{hh} + \frac{N_0}{2}\left(\boldsymbol{X}_{\mathrm{LT}}\boldsymbol{X}_{\mathrm{LT}}^{\mathsf{H}}\right)^{-1}\right)^{-1}\hat{\boldsymbol{h}}_{\mathrm{LT-LS}}, \tag{3.6}$$

where $\boldsymbol{R}_{hh} = E\{\boldsymbol{h}\boldsymbol{h}^{\mathsf{H}}\}$ is the channel autocorrelation. In the above expression, it has been assumed that the channel frequency responses $\boldsymbol{h}_1$ and $\boldsymbol{h}_2$ are approximately equal. If $\boldsymbol{R}_{hh}$, $\boldsymbol{X}_{\mathrm{LT}}$, and N_0 are known beforehand, the estimator matrix can be precomputed and stored.

The block LS and LMMSE channel estimates are used for detecting the data over the rest of the frame. These methods are suitable when the variation of the channel over the frame duration is insignificant.

In [42, Sec. 4.3], LMMSE interpolation is described for channel estimation where channel estimate at a data symbol position is obtained as a linear combination of LS channel estimates at the pilot positions. The LS channel estimates at pilot positions are arranged in a vector $\hat{\boldsymbol{h}}_{\mathrm{p}}$ and the channel coefficients to be estimated in the vector form $\hat{\boldsymbol{h}}_{\mathrm{d}}$ are given by

$$\hat{\boldsymbol{h}}_{\mathrm{d}} = \boldsymbol{R}_{\mathrm{dp}}\boldsymbol{R}_{\mathrm{pp}}^{-1}\hat{\boldsymbol{h}}_{\mathrm{p}}, \tag{3.7}$$

where $\boldsymbol{R}_{\mathrm{dp}} = E\{\hat{\boldsymbol{h}}_{\mathrm{d}}\hat{\boldsymbol{h}}_{\mathrm{p}}^{\mathsf{H}}\}$ and $\boldsymbol{R}_{\mathrm{pp}} = E\{\hat{\boldsymbol{h}}_{\mathrm{p}}\hat{\boldsymbol{h}}_{\mathrm{p}}^{\mathsf{H}}\}$. In the same work, low rank approximations based on single value decomposition are discussed to reduce the complexity of the estimators in (3.6) and (3.7).

3.2.2 Decision Feedback

Decision feedback based channel estimation schemes can be utilized to alleviate the problem of channel estimation due to the ill-suited pilot pattern. Decision feedback methods for 802.11p employ pilot aided channel estimation schemes to obtain channel estimates at the beginning of the frame and use these estimates to make decisions on bits or symbols. Consequently, the decisions are used to update the initial channel estimates. Figure 3.2 shows the schematic structures of generic decision feedback estimators where the decisions on symbols, and data bit decisions or a-posteriori probabilities (APPs) of the coded bits are used for updating the channel estimates.

In [17], an early work on supporting mobility in 802.11a, a decision directed channel estimation scheme is proposed. The data bits detected at the output of the channel

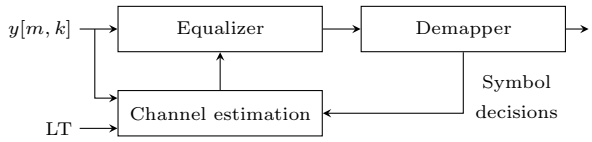

(a) Constellation aided

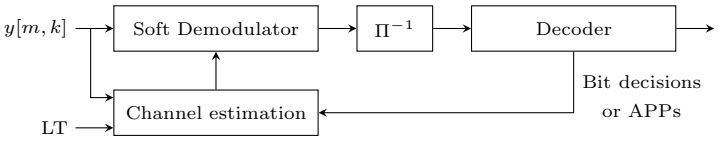

(b) Bit decision aided

Figure 3.2: Schematic structures of decision feedback channel estimators.

decoder using the initial channel estimates are reencoded, reinterleaved, and remapped to regenerate the transmitted constellation symbols. Assuming error free detection from the channel decoder, the regenerated complex symbols are treated as pilot symbols and the corresponding received symbols are used to obtain new channel estimates. The new channel estimates and the previous channel estimates are combined using different weights to compute updated channel estimates. The optimal weights were determined empirically for a specific channel model, update rate, and signal-to-noise ratio (SNR).

A decision directed channel estimation scheme referred to as spatial temporal averaging (STA) is described in [19]. In STA, initial channel estimates obtained from the LT symbols are used to make a decision on the transmitted constellation symbols of the following received OFDM symbol. The decided symbols are then used to obtain new channel estimates. The new channel estimates are averaged in frequency and in time with weights determined from channel characteristics to form updated channel estimates. In comparison to the method in [17], STA does not use the decoded bits to regenerate the transmitted constellation symbols and is hence computationally less complex. A channel estimation scheme named constructed data pilot (CDP) that is based on the assumption that the channel coefficient of a received symbol is highly correlated with that of the previous symbol is proposed in [20]. In CDP, the validity of the newly computed channel estimate is determined and if it is found to be invalid, previously computed channel estimate is retained for the channel update. This step tries to prevent a wrong update of the estimate in case the symbol detected is incorrect due to noise. The STA and CDP methods show improvements in the FER performance in comparison to the block LS method. However, in [19] and [20], the FER performance of the STA and CDP schemes has not been compared against the case with perfect CSI.

Turbo equalization makes use of the turbo principle to jointly detect the data and estimate the channel [47]. A receiver structure similar to the structure shown in Figure 3.2(b), that uses turbo equalization is discussed in [23]. In turbo equalization, initial

likelihood ratios of coded bits are computed using the initial channel estimates and fed into a soft-input soft-output channel decoder. The soft-output bits are then used along with the initial channel estimates to update the channel estimates. The process of decoding and updating the channel estimates is iterated until a certain stopping criterion is met. An iterative channel estimation scheme that uses generalized discrete prolate spheroidal sequences is shown to provide FER performance very close to the case with perfect CSI in [22]. It has also been shown in the same work that the number of iterations required can be reduced by introducing a postamble at the end of the frame. A factor graph based iterative receiver with reduced complexity is described in [24]. Although good FER performance is reported for varying frame lengths, the FER is still far away from the case with perfect CSI (more than 4 dB difference in SNR). Also, it is seen from the results that the number of iterations required to achieve a fixed bit error rate (BER) increases when the frame length increases. Similar to the results in [22], the number of iterations required to achieve a fixed BER in [24] is shown to reduce with the inclusion of a postamble. Both studies indicate the usefulness of more pilots to reduce latency in iterative receiver structures. Also, pilots distributed throughout the frame allow iterative equalization and detection over a smaller portion of the frame.

3.3 Cross-layered Pilot Insertion Scheme

Channel estimation schemes, such as block LS and block LMMSE, based only on the standard 802.11p pilots perform poorly in highly time- and frequency-varying channels, and the FER performance improves very slowly with SNR. The FER performance of the low complexity decision feedback methods such as STA and CDP is far from the case with perfect CSI. In case of iterative equalization, where performance close to the case with perfect CSI is obtained, the algorithms are complex. Pilots distributed throughout the frames are beneficial to perform robust channel estimation with low complexity algorithms [40]. Frame formats where the pilots are distributed throughout the frame have been proposed for vehicular communications. Three pilot patterns referred to as enhanced pilot (EP) patterns and periodically inserted pilot OFDM symbols referred to as midambles are proposed in [14]. The concept of midambles is revisited in [15], where a channel tracking algorithm using the midambles is discussed.

In the appended papers [33, 36], a cross-layered pilot insertion scheme to introduce complementary pilot OFDM symbols referred to as pseudo training (PT) symbols into the SF is proposed. In contrast to the pilot schemes introduced in [14–16], the proposed scheme is backward compatible with standard 802.11p transceivers. A modified receiver can make use of the inserted complementary training symbols for robust channel estimation. A standard receiver treats the complementary training symbols as data and passes the entire frame to the higher layers. A standard 802.11p transceiver needs a software/firmware update in the logical link control (LLC) layer that is immediately above PHY and MAC layers (that are typically implemented in hardware and cannot be modified) to insert/remove the PT symbols. Since the proposed pilot insertion scheme is backward compatible, it will provide more support for channel estimation while allowing older transceivers to co-exist.

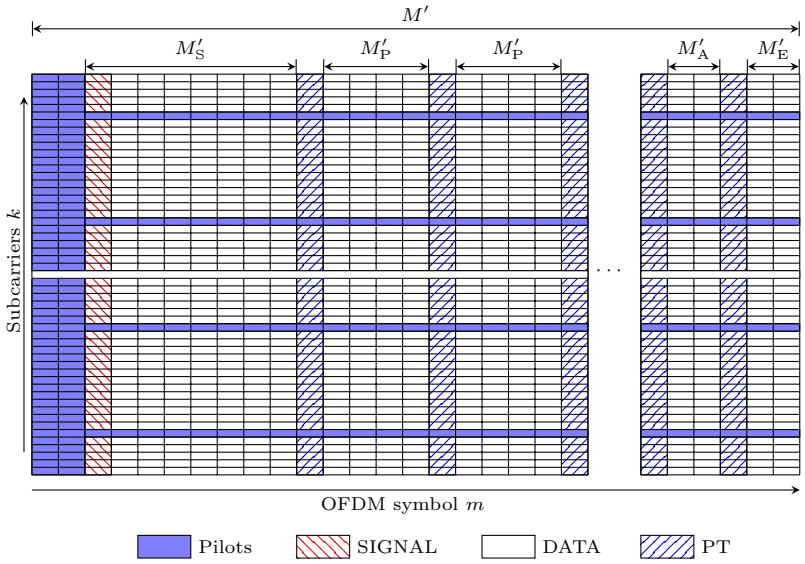

Figure 3.3: A modified 802.11p frame in subcarrier-time grid showing the position of the pilots, the data symbols and the inserted PT symbols.

The proposed modified 802.11p frame (MF) is shown in a subcarrier-time grid in Figure 3.3. The procedure to insert the PT symbols has been described in [33, 36]. The number of OFDM symbols between two periodically inserted PT symbols is denoted by M'_{P}, which is the design parameter of the MF and can be made adaptive depending on the channel conditions or the reliability requirement of an application. The number of OFDM symbols between the LT symbols and the first PT symbol is denoted by M'_{S} which in some cases can be larger than M'_{P} due to the insertion of the SIGNAL symbol, SERVICE field, and MAC header by the layers below the LLC sublayer. Also, depending on the length of data packet, the frame in the end may consist of less than M'_{P} OFDM data symbols after the periodically inserted PT symbols. In that case, one additional PT symbol is inserted after the periodically inserted training at the end of the frame. The number of OFDM symbols between the final periodically inserted PT symbol and the additional PT symbol is denoted by M'_{A}. Since the cyclic redundancy check (CRC) and the termination bits are appended to the end of the frame by the layers below the LLC layer, the frame consists of M'_{E} OFDM symbols after the final PT symbol as shown in the figure.

3.4 Comparison of Channel Estimation Schemes

The FER performances of some of the channel estimation schemes are compared in this section. The receiver and the EXP channel model described in [33] are used. The

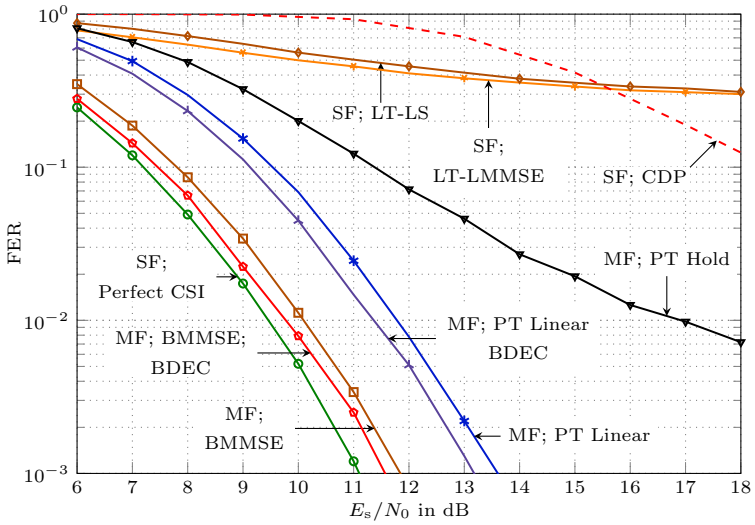

Figure 3.4: Simulation FER results of SFs ($M = 35$) and MFs ($M = 37$) for different channel estimation schemes in the EXP channel with $v = 100$ km/h.

EXP channel model is a stochastic channel model having an exponentially decaying PDP with $\tau_{\text{rms}} = 0.4\,\mu$s. The tap gains are independent zero mean complex Gaussian with autocorrelation function $\alpha_l \text{J}_0(2\pi(v/\lambda)t)$, where α_l is the average power of the lth tap, v is the relative velocity between the TX and the RX, λ is the wavelength of the electromagnetic carrier wave of frequency $f_c = 5.9\,\text{GHz}$. Hence, each tap is Rayleigh fading with the classical Clarke's power spectrum. The MCS with QPSK mapping and code rate 1/2 in [13, Table 18.4] is adopted for the safety applications and is the focus of the FER results. The FER results in this section are plotted against E_s/N_0, where E_s is the average energy of the frequency domain symbols $x[m, k]$.

Figure 3.4 shows the FER performance of different channel estimation schemes in the EXP channel with $v = 100\,\text{km/h}$. An SF with $M = 35$ OFDM symbols is transmitted. $M'_{\text{S}} = M'_{\text{P}} = 16$ is chosen for the MFs, which corresponds to $M' = 37$ in Figure 3.3 for the same length of data. The MF contains no additional PT symbol after the final periodic PT symbol and $M'_{\text{E}} = 1$. The FER of the SF in case of LT-LS and LT-LMMSE channel estimation schemes decreases very slowly with increasing SNR. Since the PT symbols are inserted periodically in an MF, two consecutive PT symbols and the data OFDM sandwiched between them can be considered as a block and channel estimation can be performed for each of the blocks separately. The block MMSE estimation (BMMSE) scheme for the MFs described in [36] that performs blockwise LMMSE interpolation has an FER performance that is close to the case with perfect CSI. However, this scheme requires the knowledge of channel correlation functions and involves large matrix operations. FERs of PT Hold and PT Linear channel estimation schemes for MFs (described in [33]) are also shown Figure 3.4. In the PT Hold scheme, the LS channel estimates at

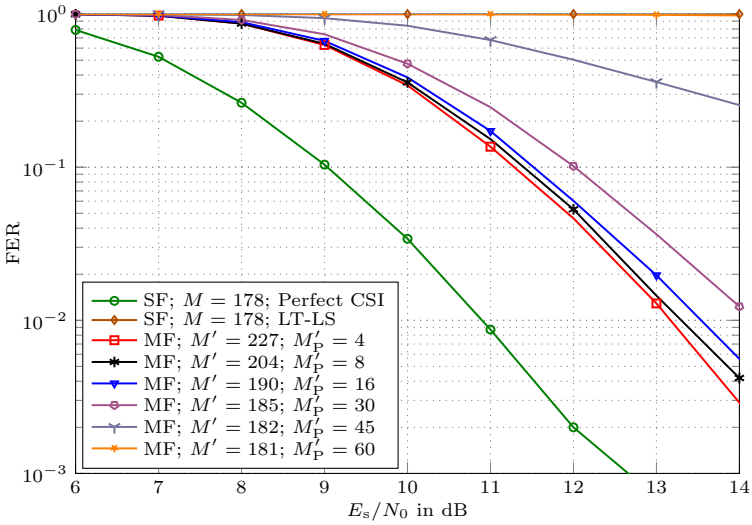

Figure 3.5: Simulation FER results of MFs using PT Linear channel estimation scheme for different M'_P in the EXP channel with $v = 200$ km/h.

a PT symbol are used for decoding the data until the next PT symbol is received. In the PT Linear scheme, the channel estimates between two consecutive PT symbols are computed using linear interpolation of the LS estimates at the PT symbols. PT Hold and PT Linear schemes are computationally simple and do not require the knowledge of the channel correlation functions. As seen in the figure, PT Linear scheme provides significant FER performance gain over the LT-LS and LT-LMMSE channel estimation schemes. The FER performance in MFs can be further improved by performing blockwise Viterbi decoding as described in [36]. The figure shows the performance improvement of the BMMSE and PT Linear schemes with block decoding (BDEC). FER performance of the CDP channel estimation scheme proposed in [20] is also shown in the figure. The FER performance of the CDP scheme improves at higher SNRs. An FER close to 10^{-2} is achieved at $E_s/N_0 = 25$ dB (not shown in the figure), which is significantly worse than in the perfect CSI case operating at around 9.5 dB.

The number of OFDM symbols between two consecutive PT symbols, M'_P, is a design parameter of the MFs. Frequent insertion of PT symbols increases the overhead of pilots. Whereas, a larger M'_P increases the buffer size required to store the data symbols between the consecutive PT symbols. Also, the FER performance provided by an M'_P is dependent on the channel estimation scheme used at the receiver. For a low complexity channel estimation scheme that does not use the channel correlation functions, or iterative decoding and equalization strategies for channel estimation, PT symbols may have to be placed more frequently than specified by the requirement stated in (3.4). Figure 3.5 shows the FER performance of the PT Linear channel estimation scheme for different values of M'_P in EXP channel with $v = 200$ km/h. An SF with $M = 178$ is transmitted,

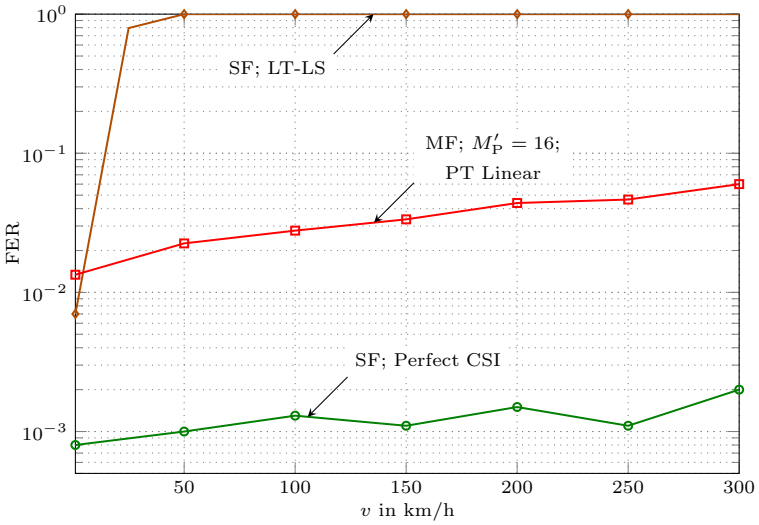

Figure 3.6: Simulation FER results of SFs with $M = 178$ and MFs with $\{M' = 190$ and $M'_P = 16\}$ for different relative velocities in EXP channel. The SNR is fixed to $E_s/N_0 = 12\,\text{dB}$.

and the lengths of the corresponding MFs are $M' = \{227, 204, 190, 185, 182, 181\}$ for $M'_P = \{4, 8, 16, 30, 45, 60\}$, respectively. The FER of the SF with LT-LS scheme is equal to 1 for all SNRs. The FER performance of the PT Linear scheme for $M'_P = \{4, 8, 16\}$ follows the performance of the SF with perfect CSI with an offset in SNR. The FER performance of the PT Linear scheme starts to degrade with $M'_P \geq 30$ and the FER is close to 1 for $M'_P = 60$. As seen in Figure 3.5, the FER performance does not improve substantially when M'_P is reduced from 16 to 4. This is due to the fact that, when the consecutive PT symbols are placed such that the channel variation between them is approximately linear, the mean squared channel estimation error in the PT Linear scheme is dominated by the estimation error of the LS estimates at the PT symbol positions and the error due to linear approximation is negligible. As a consequence, the mean squared channel estimation error in the PT Linear scheme is approximately constant when M'_P is reduced from 16 to 4, and the FER performance does not improve substantially. The PT Linear channel estimation was chosen in [33] since it is readily implemented in hardware. Other channel estimation schemes with reasonable complexity can be implemented to further improve the FER performance.

Figure 3.6 shows the FER performance as a function of relative vehicular velocity v in EXP channel at a fixed SNR, $E_s/N_0 = 12\,\text{dB}$. An SF with $M = 178$ is transmitted, and $M'_P = 16$ is chosen for the MF, which corresponds to $M' = 190$. In case of perfect CSI, the FER performance is approximately constant with increasing v. The FER of the LT-LS scheme rapidly increases to 1 with increasing v. This is due to the fact that the channel is estimated only at the beginning of the frame. The FER performance of the

PT Linear scheme slowly degrades with increasing v.

3.5 Conclusion

In this chapter, the 802.11p frame format and its pilot pattern were studied. A brief overview of the channel estimation schemes studied in literature for the 802.11p systems was given. The modified frame format with complementary training symbols, which is the result of the cross-layered pilot schemes proposed in the appended papers was introduced. Finally, the FER performances of some of the channel estimation schemes were compared. It was shown through simulations that the modified frames can provide good FER performance with low complexity channel estimation schemes for a suitably chosen period of pilot insertion.

Chapter 4

Hardware Implementation

A modified receiver capable of utilizing the complementary training symbols in MFs is implemented in HIRATE, an FPGA based hardware platform developed at Fraunhofer Heinrich Hertz Institute, Berlin [48]. The architecture of the hardware platform is described briefly in [33]. The modified receiver was implemented by extending an existing HIRATE implementation of a standard compliant 802.11p transceiver. FER measurements have been performed by interfacing the implemented transceiver with a channel emulator. Also, the backward compatibility of the pilot insertion scheme was verified by testing the implemented transceiver with a commercial 802.11p transceiver. The FER results and the verification of backward compatibility have been discussed in [33].

In this chapter, some aspects of hardware implementation that have not been included in [33] are discussed. This chapter points out some generic differences between high level language (HLL) computer simulations and FPGA implementations to communication engineers with no prior experience in FPGA implementation. The content of the chapter is based on the author's limited experience, an experienced FPGA developer might find it trivial.

4.1 Graphical Development

The HIRATE platform is based on a Gidel Procstar III evaluation board with four Altera Stratix FPGAs. The implementation of the transceiver was done in Simulink and MATLAB using a graphical design approach. Altera DSP builder provides a library of standard and advanced blocks in the Simulink environment that can be used to implement the transceiver digital signal processing (DSP) algorithms. The library includes fast Fourier transform (FFT), inverse-FFT, and soft-input Viterbi decoder blocks, which enable rapid prototyping of an 802.11p transceiver. Signals generated during the run time of the Simulink model can be exported to MATLAB-workspace allowing a user to analyze the signals using MATLAB. After the completion and verification of the Simulink model, it is then converted to hardware description language (HDL) targeted for a wide range of Altera FPGA models with the Altera signal compiler. Similar libraries and

development methodologies are supported by other FPGA vendors.

4.2 Transition from High Level Language Simulations to FPGA Implementation

Although graphical development requires little or no knowledge of HDLs, FPGA implementation differs from the HLL computer simulations significantly in some aspects. A brief description of the major differences is given below.

1. Parallel/pipeline processing: The system to be implemented in an FPGA platform has to be designed for parallel/pipeline processing. As a first step in transition from HLL simulations to FPGA implementation, the system has to be rearranged to function in parallel/pipeline processing.

2. Indexing: HLLs used for the simulations offer a large flexibility in indexing arrays and matrices. However, in an FPGA implementation, indexing involves usage of counters to generate indices or prestorage of indices in the read only memory (ROM) space.

3. Precision: All the signals in an FPGA implementation have finite and varying bit widths. Using the same precision as in the FPGA implementation for all the variables in the HLL simulations would be helpful in including the effects of limited precision on algorithms.

4. Processing delay: A signal processing operation in an FPGA requires a fixed number of clock cycles and hence the output of the operation is delayed. Owing to the pipelined nature of the implementation, delay introduced by a processing block has to be taken into consideration. Any other signals that are to be processed together with the output of the operation have to be aligned in time according to the delay.

5. Memory: Any signal that cannot be immediately fed to a block for further processing has to be delayed or stored for accessing later. Storing and reading involves generating indices and signals for writing/reading from random access memories (RAMs).

6. Registers: Registers are used to add flexibility into an FPGA implementation. The content of the registers can be changed during the run time of the implementation. Registers allow us to change the operation mode of the implementation or make the constants used in algorithms adaptive. However, the implementation should already include all the elements necessary to adapt according to the values in the registers.

7. Completeness: In baseband HLL simulations of digital communications, frame detection, synchronization, and automatic gain control (AGC) are assumed to be perfect. This is a good abstraction for developing algorithms. Nonetheless, if the

end goal is the development and verification of a complete FPGA transceiver implementation, it is necessary to include all the receiver front end operations in the simulations to capture the influence of these operations on the performance of the system.

8. Compilation and emulation: Unlike the compilation of HLLs, the compilation of an FPGA implementation is a tedious task. Care must be taken during the implementation and the design must be thoroughly verified using emulations before the compilation. However, emulation of an entire model, for example an 802.11p receiver, can be very slow since every element in the implementation is emulated for each clock cycle. This makes the verification of the model using statistical metrics such as BER and FER a tedious task.

4.3 Analog Components

A brief account of some of the analog components used in the transceiver implementation is given in this section.

1. Analog to digital converters (ADCs) and digital to analog converters (DACs): The ADCs and DACs that interface the FPGA inputs/outputs with the analog components have limited bit widths and hence, limited precision and dynamic range. HIRATE uses DACs and ADCs of 16 and 8 bit, respectively.

2. Upsampling and downsampling: The baseband algorithms operate at a sampling rate of 10 MS/s. At the transmitter, the baseband samples at 10 MS/s are upsampled to 160 MS/s, filtered using an FIR filter and then fed to the DAC. At the receiver, the output of the ADC sampled at 160 MS/s is filtered using an FIR filter and downsampled to 10 MS/s.

3. AGC: In the receiver, the ADC has a limited bit width and as a consequence, a limited dynamic range. A disadvantage of OFDM communication systems is the high peak to average power ratio (PAPR). The gain of the AGC has to be adjusted such that the clipping of the peaks and loss of smaller values is minimized. The AGC is configured to control the gain of the amplifier such that the average signal power is at a certain dB level with reference to the full scale of the ADC, denoted by dBFS.

4. Other analog components such as reference clocks, oscillators, up- and down-mixers, and amplifiers also have a huge influence on the performance of the final transceiver implementation. The author has not worked with these components and hence refrains from describing them. Poor electromagnetic shielding of cables and wear-and-tear of connectors can also have undesired effects on the performance and the repeatability of the experiments.

4.4 Challenges and Correction Measures

Some of the challenges encountered during the implementation and measurement, and the measures taken to overcome them are briefly discussed in this section.

1. Debugging: When a change is made to an FPGA implementation, the HDL code has to be regenerated and reintegrated into the entire design for testing on the FPGA platform. If the implementation is large, for example a complete 802.11p receiver, the HDL code generation and integration takes a long time. Therefore, it is necessary to take suitable measures during implementation of a feature so that it can be verified during the execution on FPGA. In HLL simulations, all the intermediate signals can be easily stored and analyzed for errors. However, in an FPGA implementation, if a signal needs to be debugged it has to be stored in the RAM while it is valid during the run time and read later on for debugging. As a consequence, during the implementation of a feature, it is also necessary to implement storing and reading of signals relevant for debugging.

2. Switches: In an FPGA implementation, various blocks of the system are interlinked and designed to work in a parallel/pipeline mode. A newly added feature might render the implementation nonfunctional. To be able to firmly conclude that the problem is due to the newly added feature, it is desirable to have an option for disabling the feature after the final compilation has been done. This can be done by including switches and multiplexers to enable/disable the feature.

3. Measurements: When measurements are performed with the analog components it is important to isolate the interference among the components. Undesired interference among analog components can result in unexpected results and make the verification of the signal processing algorithms a challenging task.

4.5 Updates to the Existing Implementation

A receiver capable of utilizing the inserted training symbols was implemented by modifying an existing HIRATE 802.11p implementation. The most important additions and/or modifications performed are listed below.

1. Soft demodulator: The existing implementation used hard decision for demapping the received QPSK symbols to bits. The hard decision is replaced to compute max-log approximations of log-likelihood ratios (LLRs) of the coded bits.

2. Viterbi decoder: Since hard decision was used for demapping, a binary-input Viterbi decoder was used for decoding. The binary-input decoder is replaced with a soft-input Viterbi decoder with a bit width of 16 bits for each of the two soft inputs (a rate 1/2 convolutional code is used). The Viterbi decoder is available as a preimplemented block in the DSP builder library. The max-log LLRs are scaled and clipped to be accommodated in 16 bits.

3. Generate inserted training symbols: For generating the inserted training symbols at the receiver, the procedure described in [33, 36] is implemented. The initial LS estimates computed from LT are used to compute the LLRs of coded bits in the first several OFDM symbols and to decode the SERVICE field that consists of scrambler initialization and M'_{P}. Using the scrambler initialization, M'_{P}, and the training sequence inserted, the inserted PT symbols are generated.

4. Channel estimation: The existing implementation used the LS channel estimates computed using the LT symbols for equalizing the received symbols for the entire frame. The implementation is updated to use the generated PT symbols. The PT symbols are used to compute LS channel estimates at the PT symbol positions. These channel estimates are utilized using either the PT Hold or the PT Linear channel estimation schemes described in [33].

4.6 Conclusion

With the recent developments in the graphical tools for FPGA implementation, it is possible for an algorithm developer with limited knowledge of HDLs to implement and verify algorithms on an FPGA platform. However, there exist many differences between commonly used HLL simulations for algorithm verification and FPGA implementation. In this chapter, some of the important differences were highlighted.

Chapter 5

Contributions and Conclusions

5.1 Contributions

This thesis studies the problem of channel estimation in vehicular communications in the context of the 802.11p standard, whose pilot pattern is ill-suited for the highly time- and frequency-varying wireless vehicular channels. The contributions made by the author, to alleviate the problem of ill-suited pilot pattern, are presented in Part II of the thesis in the form of two papers summarized below.

5.1.1 Paper A: "On Channel Estimation for 802.11p in Highly Time-Varying Vehicular Channels"

In Paper A, a cross-layered pilot insertion scheme to insert complementary pilots into the 802.11p frame is proposed. The proposed scheme enables the insertion of pilots above the MAC layer and hence allows a standard transmitter to transmit modified frames with the complementary pilots. A modified receiver can utilize the inserted pilots for robust channel estimation. A standard receiver sees the additional pilots as data and passes them to the higher layers, where they are removed. A modified receiver that performs robust channel estimation utilizing the inserted complementary pilots and LMMSE interpolation is described. Blockwise LMMSE interpolator that performs LMMSE interpolation in blocks is also discussed to reduce the complexity of the LMMSE interpolation. Numerical results show that FER performance close to the case with perfect CSI is achieved with blockwise LMMSE interpolation for a suitably chosen period for pilot insertion.

5.1.2 Paper B: "An 802.11p Cross-layered Pilot Scheme for Time- and Frequency-Varying Channels and Its Hardware Implementation"

In Paper B, the procedure to insert complementary training symbols proposed in Paper A is further improved to include support for short frames. Two low complexity channel

estimation schemes that utilize the inserted pilots in modified frames for improved channel estimation are presented. The hardware implementation feasibility of the proposed scheme is shown by implementing a modified receiver in an FPGA platform. Also, the backward compatibility of the proposed scheme is verified by performing compatibility tests with a standard compliant commercial 802.11p transceiver. FER measurements are performed by interfacing the FPGA implementation with a channel emulator. FER performance of the modified receiver follows the performance of a receiver with the knowledge of perfect CSI with an offset of 3.5 to 4 dB in SNR for a suitably chosen period of pilot insertion, and the modified receiver significantly outperforms the commercial 802.11p transceiver we tested.

5.2 Conclusions

In this thesis, an 802.11p backward-compatible cross-layered pilot scheme was proposed to provide more support for channel estimation in highly time- and frequency-varying vehicular channels. The iterative schemes studied in the literature overcome the problem of the ill-suited pilot pattern in 802.11p frames at the cost of increased receiver complexity and hence, the cost of the transceiver chipsets. At present, the 802.11p standard is not undergoing any modification to include more pilots for aiding in channel estimation. The proposed pilot scheme is not specific to a receiver structure and receivers with reasonable complexity can be implemented to utilize the complementary pilots in the modified frames. Considering these factors, the pilot scheme proposed in this thesis provides a means to design and manufacture low-complexity low-cost transceivers, or to even aid the iterative schemes in reducing the complexity and the number of iterations required to achieve a required FER performance.

References

[1] "Intelligent transport systems (ITS); vehicular communications; basic set of applications; definitions," *ETSI TR 102 638 (V1.1.1)*, 2009.

[2] D. Eckhoff, B. Halmos, and R. German, "Potentials and limitations of green light optimal speed advisory systems," in *IEEE Vehicular Networking Conference*, Boston, MA, USA, Dec. 2013, pp. 103–110.

[3] C. Mecklenbräuker, A. F. Molisch, J. Karedal, F. Tufvesson, A. Paier, L. Bernadó, T. Zemen, O. Klemp, and N. Czink, "Vehicular channel characterization and its implications for wireless system design and performance," *Proceedings of the IEEE*, vol. 99, no. 7, pp. 1189–1212, July 2011.

[4] G. Acosta-Marum and M. Ingram, "Doubly selective vehicle-to-vehicle channel measurements and modeling at 5.9 GHz," in *International Symposium on Wireless Personal Multimedia Communications*, San Diego, CA, USA, 2006.

[5] D. Matolak, I. Sen, and W. Xiong, "Channel modeling for V2V communications," in *Third Annual International Conference on Mobile and Ubiquitous Systems: Networking Services*, San Jose, CA, USA, July 2006, pp. 1–7.

[6] G. Acosta-Marum and M. Ingram, "Six time- and frequency-selective empirical channel models for vehicular wireless LANs," *IEEE Vehicular Technology Magazine*, vol. 2, no. 4, pp. 4–11, Dec. 2007.

[7] I. Sen and D. Matolak, "Vehicle-vehicle channel models for the 5-GHz band," *IEEE Transactions on Intelligent Transportation Systems*, vol. 9, no. 2, pp. 235–245, June 2008.

[8] A. Paier, "The vehicular radio channel in the 5 GHz band," Ph.D. dissertation, Institut für Nachrichtentechnik und Hochfrequenztechnik (E389), Vienna University of Technology, Oct. 2010.

[9] L. Bernadó, T. Zemen, F. Tufvesson, A. F. Molisch, and C. Mecklenbräuker, "Delay and Doppler spreads of nonstationary vehicular channels for safety-relevant scenarios," *IEEE Transactions on Vehicular Technology*, vol. 63, no. 1, pp. 82–93, Jan. 2014.

[10] T. Abbas, "Measurement based channel characterization and modeling for vehicle-to-vehicle communications," Ph.D. dissertation, Department of Electrical and Information Technology, Lund University, Jan. 2014.

[11] E. G. Ström, "On medium access and physical layer standards for cooperative intelligent transport systems in Europe," *Proceedings of the IEEE*, vol. 99, no. 7, pp. 1183–1188, July 2011, Invited paper.

[12] J. B. Kenney, "Dedicated short-range communications (DSRC) standards in the United States," *Proceedings of the IEEE*, vol. 99, no. 7, pp. 1162–1182, July 2011, Invited paper.

[13] "Wireless LAN medium access control (MAC) and physical layer (PHY) specifications," *IEEE Std 802.11-2012*, pp. 1–2793, 2012.

[14] R. Grünheid, H. Rohling, J. Ran, E. Bolinth, and R. Kern, "Robust channel estimation in wireless LANs for mobile environments," in *IEEE Vehicular Technology Conference*, Vancouver, BC, Canada, Sept. 2002, pp. 1545–1549.

[15] W. Cho, S. I. Kim, H.-K. Choi, H.-S. Oh, and D.-Y. Kwak, "Performance evaluation of V2V/V2I communications: The effect of midamble insertion," in *1st International Conference on Wireless Communication, Vehicular Technology, Information Theory and Aerospace Electronic Systems Technology*, Aalborg, Denmark, May 2009, pp. 793–797.

[16] S. Sibecas, C. Corral, S. Emami, G. Stratis, and G. Rasor, "Pseudo-pilot OFDM scheme for 802.11a and R/A in DSRC applications," in *IEEE Vehicular Technology Conference*, Orlando, FL, USA, Oct. 2003, pp. 1234–1237.

[17] T. Kella, "Decision-directed channel estimation for supporting higher terminal velocities in OFDM based WLANs," in *IEEE Global Telecommunications Conference*, San Francisco, CA, USA, Dec. 2003, pp. 1306–1310.

[18] J. Fernandez, D. Stancil, and F. Bai, "Dynamic channel equalization for IEEE 802.11p waveforms in the vehicle-to-vehicle channel," in *Allerton Conference on Communication, Control, and Computing*, Allerton, IL, USA, Sept. 2010, pp. 542–551.

[19] J. Fernandez, K. Borries, L. Cheng, B. Kumar, D. Stancil, and F. Bai, "Performance of the 802.11p physical layer in vehicle-to-vehicle environments," *IEEE Transactions on Vehicular Technology*, vol. 61, no. 1, pp. 3–14, Jan. 2012.

[20] Z. Zhao, X. Cheng, M. Wen, B. Jiao, and C.-X. Wang, "Channel estimation schemes for IEEE 802.11p standard," *IEEE Intelligent Transportation Systems Magazine*, vol. 5, no. 4, pp. 38–49, Oct. 2013.

[21] Z. Zhao, X. Cheng, M. Wen, L. Yang, and B. Jiao, "Constructed data pilot-assisted channel estimators for mobile environments," *IEEE Transactions on Intelligent Transportation Systems*, vol. 16, no. 2, pp. 947–957, Apr. 2015.

[22] T. Zemen, L. Bernadó, N. Czink, and A. F. Molisch, "Iterative time-variant channel estimation for 802.11p using generalized discrete prolate spheroidal sequences," *IEEE Transactions on Vehicular Technology*, vol. 61, no. 3, pp. 1222–1233, Mar. 2012.

[23] P. Alexander, D. Haley, and A. Grant, "Cooperative intelligent transport systems: 5.9-GHz field trials," *Proceedings of the IEEE*, vol. 99, no. 7, pp. 1213–1235, July 2011.

[24] O. Goubet, G. Baudic, F. Gabry, and T. J. Oechtering, "Low-complexity scalable iterative algorithms for IEEE 802.11p receivers," *IEEE Transactions on Vehicular Technology*, vol. 64, no. 9, pp. 3944–3956, Sept. 2015.

[25] A. Goldsmith, *Wireless communications*. Cambridge University Press, 2005.

[26] A. Molisch, *Wireless Communications*, ser. Wiley-IEEE. Wiley, 2010. [Online]. Available: https://books.google.se/books?id=vASyH5-jfMYC

[27] D. Tse and P. Viswanath, *Fundamentals of Wireless Communication*. Cambridge University Press, 2005.

[28] J. Kunisch and J. Pamp, "Wideband car-to-car radio channel measurements and model at 5.9 GHz," in *IEEE Vehicular Technology Conference*, Calgary, BC, Canada, Sept. 2008, pp. 1–5.

[29] J. Karedal, N. Czink, A. Paier, F. Tufvesson, and A. Molisch, "Path loss modeling for vehicle-to-vehicle communications," *IEEE Transactions on Vehicular Technology*, vol. 60, no. 1, pp. 323–328, Jan. 2011.

[30] L. Reichardt, J. Maurer, T. Fügen, and T. Zwick, "Virtual drive: A complete V2X communication and radar system simulator for optimization of multiple antenna systems," *Proceedings of the IEEE*, vol. 99, no. 7, pp. 1295–1310, July 2011.

[31] G. Matz, "On non-WSSUS wireless fading channels," *IEEE Transactions on Wireless Communications*, vol. 4, no. 5, pp. 2465–2478, 2005.

[32] "Car-2-car communication consortium task force antannae and wireless performance-whitepaper (ver 1.2)." Tech. Rep., Oct. 2014.

[33] K. K. Nagalapur, F. Brännström, E. G. Ström, F. Undi, and K. Mahler, "An 802.11p cross-layered pilot scheme for time- and frequency-varying channels and its hardware implementation," *submitted to IEEE Transactions on Vehicular Technology, Connected Vehicle Series*, 2015.

[34] J. Karedal, F. Tufvesson, N. Czink, A. Paier, C. Dumard, T. Zemen, C. Mecklenbräuker, and A. Molisch, "A geometry-based stochastic MIMO model for vehicle-to-vehicle communications," *IEEE Transactions on Wireless Communications*, vol. 8, no. 7, pp. 3646–3657, July 2009.

[35] A. Molisch, "A generic model for MIMO wireless propagation channels in macro- and microcells," *IEEE Transactions on Signal Processing*, vol. 52, no. 1, pp. 61–71, Jan. 2004.

[36] K. K. Nagalapur, F. Brännström, and E. G. Ström, "On channel estimation for 802.11p in highly time-varying vehicular channels," in *IEEE International Conference on Communications (ICC)*, Sydney, Australia, June 2014, pp. 5659–5664.

[37] "Intelligent transport systems (ITS); European profile standard for the physical and medium access control layer of intelligent transport systems operating in the 5 GHz frequency band," *ETSI ES 202 663 (V1.1.0)*.

[38] Y. Li and G. L. Stuber, *Orthogonal Frequency Division Multiplexing for Wireless Communications*. Springer Science & Business Media, 2006.

[39] U. Madhow, *Fundamentals of Digital Communication.* Cambridge University Press, 2008.

[40] P. Hoeher, S. Kaiser, and P. Robertson, "Two-dimensional pilot-symbol-aided channel estimation by Wiener filtering," in *IEEE International Conference on Acoustics, Speech, and Signal Processing*, Munich, Germany, Apr. 1997, pp. 1845–1848.

[41] J.-J. van de Beek, O. Edfors, M. Sandell, S. K. Wilson, and P. O. Börjesson, "On channel estimation in OFDM systems," in *IEEE Vehicular Technology Conference*, vol. 2, Chicago, IL, USA, July 1995, pp. 815–819.

[42] O. Edfors, "Low-complexity algorithms in digital receivers," Ph.D. dissertation, Luleå Tekniska Universitet, 1996.

[43] M. Sandell, "Design and analysis of estimators for multicarrier modulation and ultrasonic imaging," Ph.D. dissertation, Luleå Tekniska Universitet, 1996.

[44] O. Edfors, M. Sandell, J.-J. van de Beek, S. K. Wilson, and P. O. Börjesson, "OFDM channel estimation by singular value decomposition," in *IEEE Vehicular Technology Conference*, Atlanta, GA, USA, Apr. 1996, pp. 923–927.

[45] Y. Li, "Pilot-symbol-aided channel estimation for OFDM in wireless systems," *IEEE Transactions on Vehicular Technology*, vol. 49, no. 4, pp. 1207–1215, July 2000.

[46] H. Minn and V. Bhargava, "An investigation into time-domain approach for OFDM channel estimation," *IEEE Transactions on Broadcasting*, vol. 46, no. 4, pp. 240–248, Dec. 2000.

[47] C. Douillard, M. Jézéquel, C. Berrou, A. Picart, P. Didier, and A. Glavieux, "Iterative correction of intersymbol interference: Turbo-equalization," *European Transactions on Telecommunications*, vol. 6, no. 5, pp. 507–511, 1995.

[48] "High performance digital radio testbed (HIRATE)," http://www.hhi.fraunhofer.de/departments/wireless-communications-and-networks/research-areas/enabling-technologies-for-future-wireless-applications/hirate-high-performance-digital-radio-testbed.html, Accessed: 2015-09-23.